

CrystEngComm

Accepted Manuscript



This is an *Accepted Manuscript*, which has been through the Royal Society of Chemistry peer review process and has been accepted for publication.

Accepted Manuscripts are published online shortly after acceptance, before technical editing, formatting and proof reading. Using this free service, authors can make their results available to the community, in citable form, before we publish the edited article. We will replace this *Accepted Manuscript* with the edited and formatted *Advance Article* as soon as it is available.

You can find more information about *Accepted Manuscripts* in the [Information for Authors](#).

Please note that technical editing may introduce minor changes to the text and/or graphics, which may alter content. The journal's standard [Terms & Conditions](#) and the [Ethical guidelines](#) still apply. In no event shall the Royal Society of Chemistry be held responsible for any errors or omissions in this *Accepted Manuscript* or any consequences arising from the use of any information it contains.

One-Step Template-Free Synthesis of Hollow Core–Shell α -Fe₂O₃ Microspheres with Improved Lithium Storage and Gas-Sensing Properties

Haojie Song^{1*}, Tao Chen¹, Xueqiang Zhang¹, Xiaohua Jia²

¹ School of Materials Science and Engineering, Jiangsu University, Zhenjiang, Jiangsu, 212013,
China

² School of Environment and Safety Engineering, Jiangsu University, Zhenjiang, Jiangsu, 212013,
China

Abstract

Hollow core–shell α -Fe₂O₃ microspheres were easily prepared by one pot hydrothermal method without employing any templates/substrates or surfactants. The as-prepared samples were characterized by X-ray diffraction (XRD), scanning electron microscope (SEM), transmission electron microscope (TEM), nitrogen adsorption-desorption isotherms. Results showed that the shell was constructed by aggregated α -Fe₂O₃ nanoparticles, while the core presented a novel porous structure. The morphology of the hollow core–shell α -Fe₂O₃ microspheres can be controlled by optimizing the experimental conditions. A possible formation mechanism was also proposed. As anodes in lithium ion cells, the hollow core–shell α -Fe₂O₃ microspheres show high initial discharge capacity of 1465 mA h g⁻¹ and still a rather high capacity of 728 mA h g⁻¹ after 60 cycles. When applied as gas sensors, the hollow core–shell α -Fe₂O₃ microspheres exhibited high gas sensitivity toward NO₂ gas. The intrinsic hollow core–shell nature as well as high porosity of the core contributes greatly to improved performance as anode materials for lithium ion batteries and the superior

*To whom Correspondence should be addressed. E-mail address: songhj@ujs.edu.cn.
Tel.: +86-511-88790191. Fax: +86-511-88780191

sensitivities to NO₂ gas.

Keywords: Core-shell; Hollow α -Fe₂O₃ microspheres; Template-free; Lithium storage; Gas-Sensing;

1. Introduction

α -Fe₂O₃ (hematite), an environmentally friendly n-type semiconductor ($E_g = 2.1$ eV), is the most stable iron oxide under ambient conditions. It has been extensively investigated in catalysts, gas sensors, optical devices, lithium-ion batteries and electromagnetic devices, owing to its nontoxicity, low processing cost, and high resistance to corrosion [1–5]. Recently, researchers have successfully prepared numerous nano- and micrometer hematite with controlled morphologies, such as 0D nanoparticles; 1D nanowires, nanorods, or nanotubes; 2D plates or sheets; and 3D microspheres and urchin- or flower-like structures, as well as hybrid composites [6–11]. Among these different morphologies, hematite with hollow core-shell structures is more attractive to researchers [12–14], because of its properties of low density, high surface area, and excellent surface permeability compared with ordinary hematite. In addition, from the point of view of sensor design, the hollow core-shell α -Fe₂O₃ hierarchical microspheres generally have a higher specific surface area, and more importantly, core-shell structures are more favorable to the diffusion of gas molecules which can effectively shorten the response/recovery time of sensors. Similarly, as a Li-ion battery anode material, large specific surface area can provide more electrochemical active sites, while porous core-shell structure can shorten the electronic diffusion length and facilitate the diffusion of electrolyte [15].

In the past few years, numerous chemical and physicochemical methods have been developed to synthesize the hollow core-shell structures, such as sol-gel method [16–17], electrostatic spray deposition [18], hydrothermal synthesis [19], and template method [20]. Among them, the template-directed synthetic method has been more widely to produce the hollow core-shell structures, which can be simply classified into the hard template method and the soft template method. The hard templates are usually mesoporous silica [21] or carbon inorganic spheres [22], and soft ones such as surfactants, long-chain polymers. Suslick et al. [23] fabricated an iron/carbon composite by using ultrasound to irradiate a mixture of carbon nanoparticles and iron pentacarbonyl in hexadecane, and then obtained hollow hematite particles by elaborately controlling the oxidation of the resulting composite. Xu et al. [24] prepared α -Fe₂O₃ hollow nanospheres by a controlled precipitation of Fe³⁺ with urea in the presence of carbonaceous saccharide nanospheres as hard templates. Zhong et al. [25] synthesized the hollow core-shell η -Fe₂O₃ microspheres through a solution process followed by a calcination treatment under ambient pressure with the assistance of PVP as a soft template. Though the template routes are definitely effective and the most common method for the fabrication of hollow core-shell structures, there are some disadvantages in template fabrication such as high cost, low yield, the possibility of product deconstruction during the template removal process, and tedious synthetic steps. Therefore, our aim is to fabricate core-shell α -Fe₂O₃ hierarchical microspheres by using a simple, controllable and template-free method.

Herein, we report a one-step template-free hydrothermal process for the

synthesis of core-shell α -Fe₂O₃ microspheres. To the best of our knowledge, there has been no report on synthesis of hollow core-shell α -Fe₂O₃ microspheres without employing any templates/substrates or surfactants. In addition, a series of electric chemical experiments and gas sensing tests were performed to compare the lithium storage capacity and gas sensitivity of the as-prepared products with different morphologies. The new process reported here affords the convenient optimization of the structure of the hollow core-shell α -Fe₂O₃ microspheres to achieve higher lithium storage and improved gas-sensing properties than the α -Fe₂O₃ solid microspheres.

2. Experimental

2.1 Synthesis of hollow core-shell α -Fe₂O₃ microspheres

All analytical grade reagents were purchased from Shanghai Chemical Reagent Ltd and were used without further purification. In a typical experiment, 30 mmol FeCl₃·6H₂O was put into 50 mL of deionized water under stirring to form a homogeneous solution. Subsequently, 50 mL of CH₃CH₂OH were introduced into the above homogeneous solution under continuous stirring. After the sample was stirred for about 30 min, the total solution was transferred into a 100 mL Teflon-lined stainless steel autoclave. The autoclave was sealed and then heated to 200 °C for 12 h. After being cooled to room temperature, the products were isolated by centrifugation, alternately washed with de-ionized water and absolute ethanol several times to remove the remaining impurities. Finally, the products were dried in air at 70 °C for 24 h. Moreover, the effect of the growth conditions, such as the volume ratio of ethanol/water, the concentration of FeCl₃, and reaction time on the morphology of

α -Fe₂O₃ structures was investigated.

2.2 Characterization

The phase structure and phase purity of the as synthesized powders were examined by X-ray diffraction (XRD, Holland Philips X'pert X-ray diffractometer with Cu-K α radiation, $\lambda=1.5406$ Å) at 40 kV, 30 mA over the 2θ range 10-80°. The general morphology of the products was examined by scanning electron microscopy (SEM) on a JEOL JSM 6700F instrument operated at 20 kV. The morphology and microstructure of the products were further investigated by transmission electron microscopy (TEM), selected area electron diffraction (SAED) patterns, and high-resolution TEM (HRTEM) using a JEOL JEM 2010F microscope working at 200 kV.

2.3 Electrochemical measurements

The electrochemical performance of the as-prepared α -Fe₂O₃ samples were tested as an anode material for lithium ion battery. The as-prepared α -Fe₂O₃ powder (50 wt.%), acetylene black (40 wt.%), and poly(vinylidene fluoride) (PVDF, 10 wt.%) were mixed in N-methyl-2-pyrrolidone (NMP) to form a slurry. The resultant slurry was pasted onto copper foil with a blade and was dried at 100°C for 12 h under vacuum conditions followed by pressing at 200 kg cm⁻². Electrochemical measurements were carried out using two-electrode coin cells with lithium metal as the counter and reference electrode. The CR2032-type coin cells were assembled in an argon-filled glove box (UniLab, Mbraun, Germany). 1 M solution of LiPF₆ dissolved in EC/DMC (1:1 volume ratio) was used as the electrolyte. The charge-discharge

measurements were measured at a current density of 150 mA g^{-1} within a voltage range of 0.1-3.0 V on a CHI-660D electrochemistry workstation.

2.4 Gas-sensing measurement

Gas-sensing properties of the as-prepared $\alpha\text{-Fe}_2\text{O}_3$ samples were measured by a computer-controlled WS-30A gas-sensing measurement system. Firstly, the $\alpha\text{-Fe}_2\text{O}_3$ samples were mixed with ethanol to form a paste and then coated onto the outside surface of an alumina tube with a diameter of 1 mm and a length of 5 mm, positioned with two Au electrodes and four Pt wires on each end of the tube. A Ni-Cr alloy filament throughout the tube was employed as a heater by tuning the heating voltage. Then, the ceramic tube was heated at $400 \text{ }^\circ\text{C}$ for 2 h to evaporate the solvent and improved the stability of the device. Before measuring the gas sensing properties, the gas sensors first was aged for several days in air. The gas sensing measurements were carried out at a working temperature increasing from 160 to $355 \text{ }^\circ\text{C}$ and 33 % relative humidity (RH). The sensing response of the gas sensor was defined as $S = R_{\text{air}}/R_{\text{gas}}$, where R_{air} and R_{gas} were the electrical resistance of the sensor in air and in the test gas, respectively. The response and recovery times were defined as the time required for a change of the resistance to reach 90 % of the equilibrium value after injecting and that for removing the detected gas, respectively.

3. Results and discussion

Fig. 1 showed a typical XRD pattern of the products obtained by a hydrothermal route at $200 \text{ }^\circ\text{C}$ for 12 h. All the detectable peaks in this pattern can be assigned to the hexagonal structure of $\alpha\text{-Fe}_2\text{O}_3$ with cell constants of $a = 0.5035 \text{ nm}$ and $c = 1.3740$

nm (JCPDS No: 33-0664). No other crystalline impurities were detected, demonstrating that the products were very high-purity and single phase. In addition, the intense and sharp diffraction peaks suggested that the as-synthesized products had a high degree of crystallization.

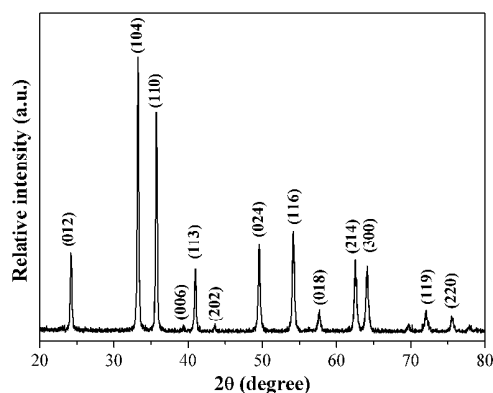


Fig. 1 XRD pattern of the products obtained at 200 °C for 12 h.

The general morphologies of the hollow core-shell α -Fe₂O₃ microspheres were observed by SEM and TEM shown in Fig. 2. Fig. 2a illuminates the synthesized powders are uniform spherical shape, with an average size of c.a. 3.0 μ m. Observation on magnified microspheres, as shown in Fig. 2b, indicates that the surface of the synthesized α -Fe₂O₃ powder is made up from nano-sized small particles. It is interesting to find that the α -Fe₂O₃ microspheres are core-void-shell structure, as evidenced by a mesosphere with partially broken shell vividly. The thickness of shell is estimated to c.a. 100 nm and the core is also made up of the same aggregated α -Fe₂O₃. Additionally, it can be seen that the surface of the core appears lots of micropore with c.a. 40 nm. The structural characterization and the hierarchical nature of the hollow core-shell α -Fe₂O₃ microspheres was further confirmed by TEM and HR-TEM observations. As shown in Fig. 2c, the high degree of contrast between the

bright region and the darker region demonstrated the circular hollow space between the shell and the core. It can be clearly distinguished that the thickness of the shell was estimated to be ca. 100 nm. Moreover, the selected area electron diffraction (SAED) patterns (inset in Fig. 2c) indicated the primary α -Fe₂O₃ nanoparticles were single-crystalline. In addition, the lattice spacing of the surface of a representative nanoparticle was measured to be 0.252 nm, which revealed that the surfaces were composed of (104) planes of α -Fe₂O₃ nanoparticles from Fig. 2d.

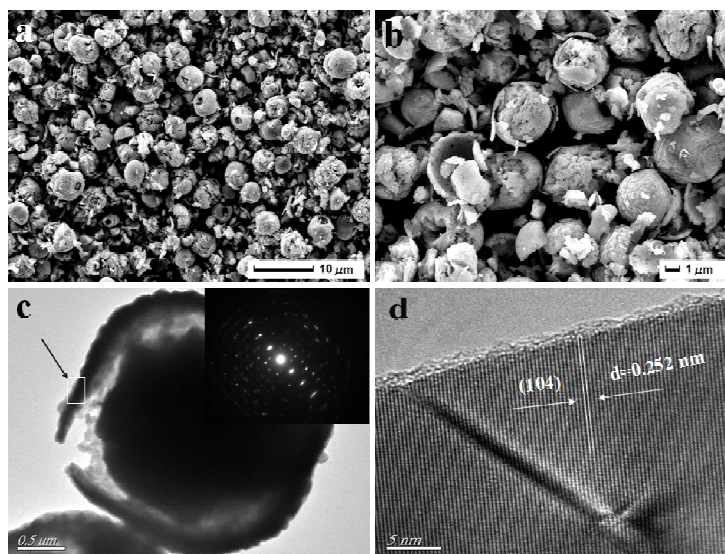


Fig. 2 (a)–(b) SEM and (c)–(d) TEM images of the hollow core–shell α -Fe₂O₃ microspheres obtained at 200 °C for 12 h. (The inset shows the SAED pattern of the sample)

The SEM images of the as-prepared α -Fe₂O₃ samples at various Fe³⁺ concentrations were shown in Fig. 3. It was found that the morphologies of samples depended strongly on the concentration of Fe³⁺. Fig. 3a is a SEM image of the sample at Fe³⁺ concentration (0.05 M), which clearly showed that around 400 nm solid particles with smooth surface are the main products. When the Fe³⁺ concentration increased to 0.1 M, the as-prepared α -Fe₂O₃ samples also have smooth surface with smaller dimension of approximately 300 nm (Fig. 3b). As the Fe³⁺ concentration

further increased up to 0.5 M, the cracked hollow core-shell α -Fe₂O₃ microspheres composed of many small nanoparticles can be observed (as shown in Fig. 3c and d).

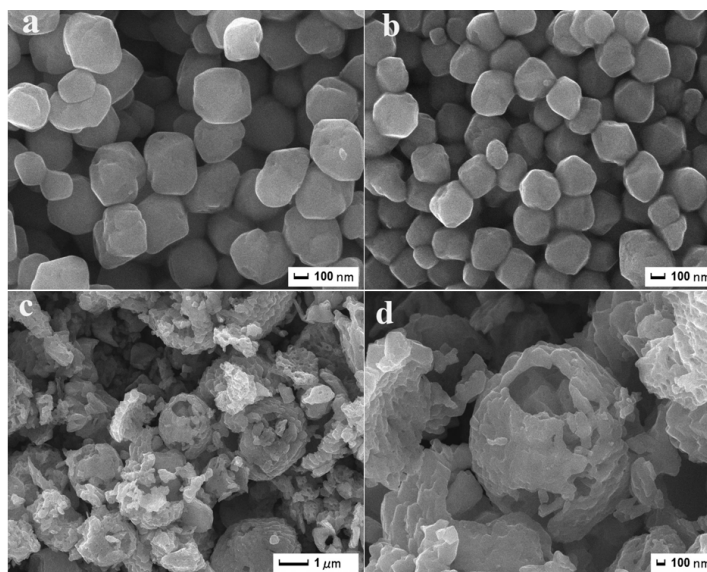


Fig. 3 SEM images of the as-prepared α -Fe₂O₃ samples obtained at 200 °C for 12 h with various Fe³⁺ concentrations: (a) 0.05 M, (b) 0.1 M, (c, d) 0.5 M.

The morphology of the as-prepared α -Fe₂O₃ samples with different volume ratios of ethanol/water was showed in Fig. 4. It was found that α -Fe₂O₃ sphere with an average diameter of 4.6 μ m had a rough surface completely existing in pure water systems (Fig. 4a). When the solvent was completely composed of alcohol, the α -Fe₂O₃ samples (Fig. 4b) are inhomogeneous spheres and have a smooth surface with a diameter ranging from 166 nm to 433 nm. As increasing the volume ratios of ethanol/water to 2:1, it is interesting that plenty of core-shell structure α -Fe₂O₃ microspheres with an average diameter of around 1.5 μ m were obtained (Fig. 4c, d).

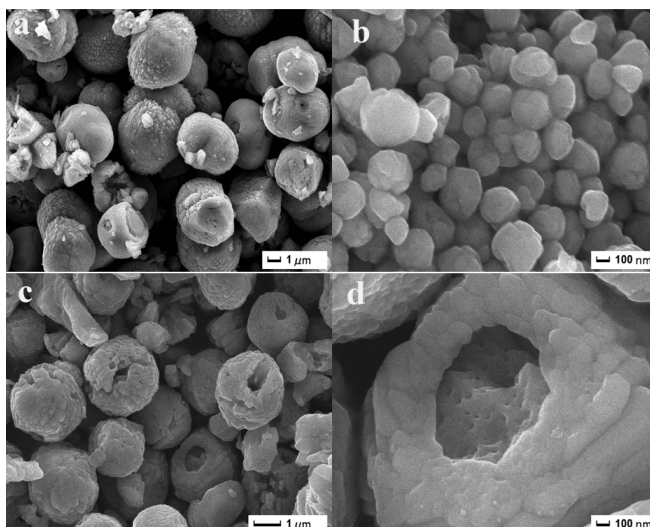


Fig. 4 SEM images of the as-prepared α -Fe₂O₃ samples obtained at 200 °C for 12 h with different volume ratios of ethanol/water: (a) no ethanol, (b) no water, (c, d) 2:1.

In order to understand the formation process of the hollow core-shell α -Fe₂O₃ microspheres, we carried out time-dependent experiments during which samples were treated with different time. SEM observations show that the products obtained for 30 min consist of nanoparticles. These nanoparticles assemble together to form loose aggregates (Fig. 5a). With increasing the reaction time, the constituent nanoparticles self-assembled further into spherelike structures as a result of oriented attachment (Fig. 5b). As the reaction went on for a longer time (6 h), integrated assembly of core-shell spheres (Fig. 5c) could be found with diameter of about 3.5 μ m. Further increasing the time to 15 h, 1.5–2.5 μ m core-shell spheres are observed (Fig. 5d). The size of spheres decreased with time increasing, which may be because of smaller crystallite dissolve into solution again.

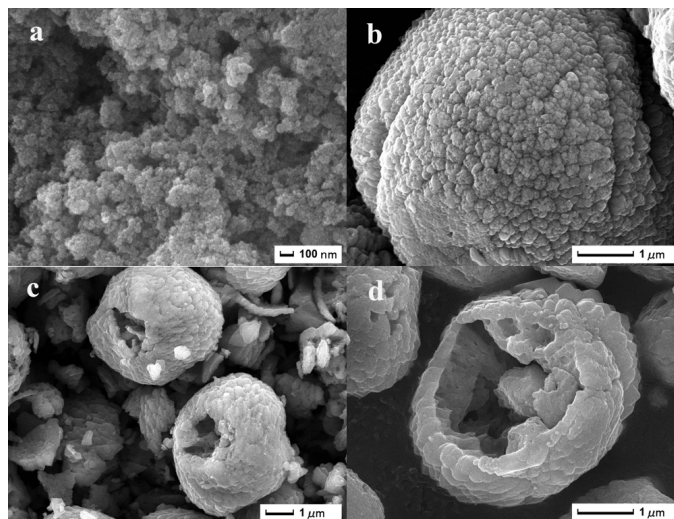


Fig. 5 SEM images of the as-prepared α -Fe₂O₃ samples obtained at 200 °C for different reaction time: (a) 0.5 h, (b) 2 h, (c) 6 h, (d) 15 h.

XRD patterns and crystallite sizes of samples prepared at different reaction time were shown in Fig. 6. When the growth time was 0.5 h, according to the main diffraction peak locations, the products could be easily indexed to a tetragonal phase of β -FeOOH (JCPDS no. 34-1266). This indicated that most of the products might be β -FeOOH. After the reaction time is further prolonged to 2 h, 6 h, and 15 h, a similar profile is obtained and all diffraction peaks can be indexed as the crystalline α -Fe₂O₃ with the hexagonal structure. No peaks of any impurities are detected in the patterns. On the basis of the width of (310) and (104) reflection, the mean size of the crystal β -FeOOH and α -Fe₂O₃ can be determined on the basis of Scherrer Equation, respectively ($D = k\lambda/\beta \cos \theta$, where $k = 0.89$, is the Scherrer constant, λ is X-ray wavelength, β is the line broadening measured at half-height, and θ is the Bragg angle of the particles). The calculated size of the crystalline was shown in Fig. 6b. It can be clearly seen that the crystallite size increase monotonically as the growth time increase.

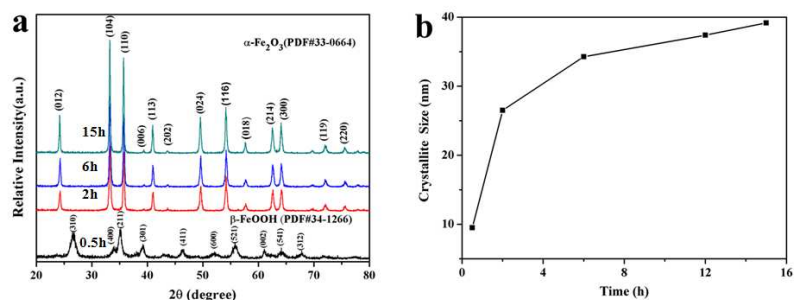
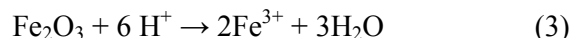
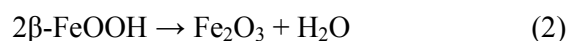


Fig. 6 XRD patterns(a) and crystallite sizes (b) of the samples prepared at different reaction time.

On the basis of the investigations described above, it is possible to interpret the formation process, which can be understood as a result of a nucleation-oriented aggregation–recrystallization mechanism from primary nanocrystals under high-temperature solvothermal conditions [26, 27]. The possible formation process of the hollow core–shell α - Fe_2O_3 microspheres is schematically illustrated in Fig. 7.



The entire solution-based growth process should be determined by the first step, as shown in the Eq. (1), at an early reaction stage, the dissolution of FeCl_3 aqueous solution yields Fe^{3+} . The formed Fe^{3+} combined with hydroxyl and became β - FeOOH . When the hydrothermal process was further prolonged, a phase transformation took place, and the precursor β - FeOOH aggregates would further dehydrate into α - Fe_2O_3 nanocrystals.[28] (Eq. (2)). Then, many neighboring freshly nanocrystals were unstable due to their high surface energy, and thus have a great tendency to spontaneously aggregate together to form solid spheres [29]. Because the initial high supersaturation results in a faster nucleation rate and the production of more

crystallites with smaller sizes, those formed small crystallites with high surface energy were wrapped in the interior of the solid spheres. In order to reduce the surface energy, these small crystallites have to dissolve and recrystallize into larger crystallites. Therefore, the dissolution primarily occurred via an Ostwald ripening process in the spheres' interior compared to exterior, eventually hollow core-shell spheres are yielded [30, 31]. During the long-drawn hydrothermal process, the presence of relatively abundant H^+ prompts the equation toward the right-hand side and enhances the degree of dissolution (Eq. (3)), which resulted in the evacuation of some holes on the cores. Finally, hollow core-shell $\alpha\text{-Fe}_2\text{O}_3$ microspheres were obtained.

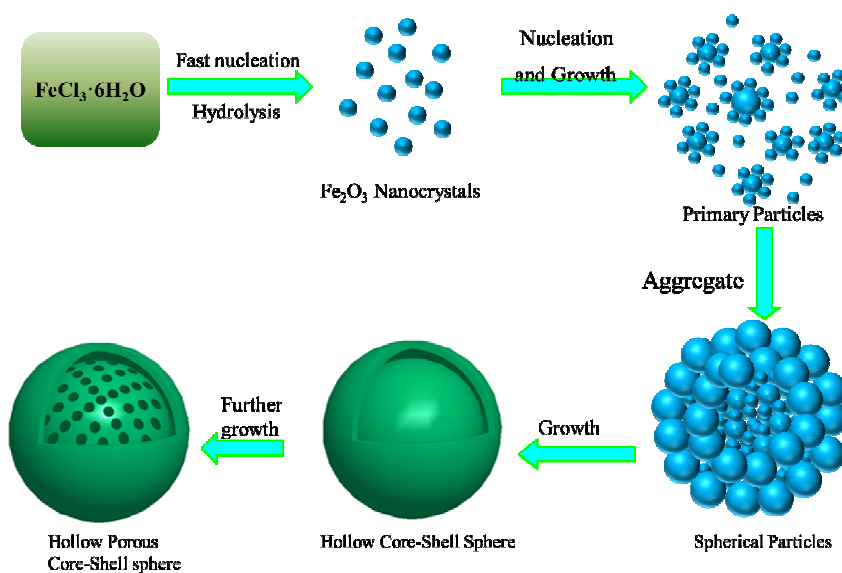


Fig. 7 Schematic illustration of the possible formation mechanism of the hollow core-shell $\alpha\text{-Fe}_2\text{O}_3$ microspheres.

The BET specific surface areas and porosity of the hollow core-shell and solid $\alpha\text{-Fe}_2\text{O}_3$ microspheres were investigated by using nitrogen adsorption and desorption isotherms in Fig. 8. The N_2 isotherms (related to the type III isotherm in the IUPAC classification) exhibit type H3 loops, indicating that the average pore size of the

hollow core-shell α -Fe₂O₃ microsphere is 27 nm in diameter (Fig. 8a). The pore size distributions observed for the hollow core-shell α -Fe₂O₃ microspheres probably reflect sample porosity related to particle dimensions comparable with pore size. However, the solid α -Fe₂O₃ microspheres have a larger pore size distribution than its dimensions, probably related to the aggregation of the microspheres (Fig. 8b). On the other hand, the measured specific surface areas of the hollow core-shell and solid structures were 62.3 m² g⁻¹, and 4.5 m² g⁻¹, respectively. These results indicate that the solid microspheres have little surface areas, while hollow core-shell microspheres have roughly large the surface area.

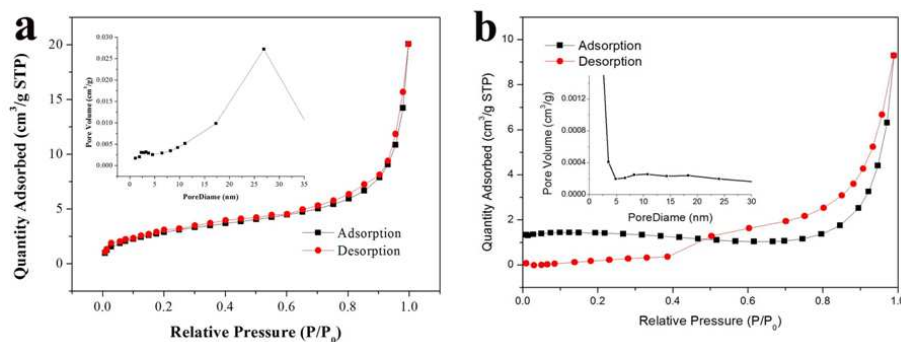


Fig.8 Nitrogen adsorption–desorption isotherms for (a) hollow core–shell α -Fe₂O₃ microspheres; (b) solid α -Fe₂O₃ microspheres.

Motivated by excellent electrochemical performance of the core-shell structure materials, here, the electrochemical characterization of the as-prepared hollow core-shell α -Fe₂O₃ microspheres for lithium storage in lithium ion batteries was evaluated by galvanostatic charge/discharge testing. As a comparison, the performances of solid α -Fe₂O₃ microspheres were also presented. Fig. 9 showed the charge/discharge voltage profiles of the hollow core-shell α -Fe₂O₃ microspheres and

the solid α -Fe₂O₃ microspheres at a current density of 150 mA g⁻¹ between voltage limits of 0.1-3.0 V (versus Li/Li⁺) on the 1st, 2nd, 3rd, 4th, and 5th cycles. The two samples showed the similar charge-discharge voltage profiles in the first cycle, which was consistent with the previous report [32]. The hollow core-shell α -Fe₂O₃ microspheres showed a higher initial discharge capacity of 1465 mAh g⁻¹ and a higher charge capacity of 956 mAh g⁻¹ than the solid α -Fe₂O₃ microspheres (discharge capacity of 1374 mAh g⁻¹ and charge capacity of 627 mAh g⁻¹) on the first cycle. The discharge and charge capacities of the hollow core-shell α -Fe₂O₃ microspheres in the 5th cycle are 899 and 875 mAh g⁻¹, respectively, which was still higher than that of the solid α -Fe₂O₃ microspheres (497 and 476 mAh g⁻¹). The 5th cyclical coulombic efficiency of the hollow core-shell α -Fe₂O₃ microspheres was 97.3 %, which was higher than the value of the solid α -Fe₂O₃ microspheres (95.7 %). The excellent Li⁺ storage performance can be attributed to the unique hollow core-shell structure. Both the core with many pores and shell are composed of small nanocrystals, possessing a high surface area, which will allow lithium ions to be introduced easily, leading to the improvement of the lithium intercalation performance.

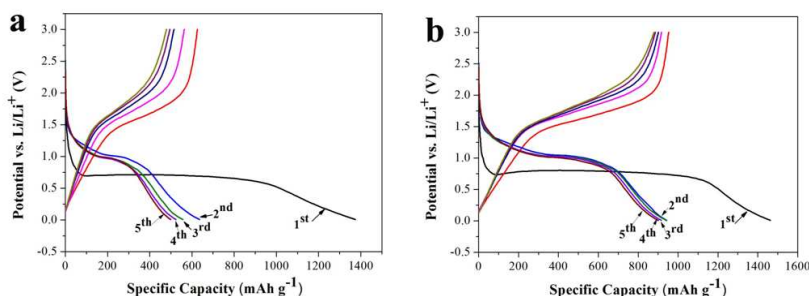


Fig. 9 The 1st, 2nd, 3rd, 4th and 5th discharge/charge voltage profiles of (a) solid α -Fe₂O₃ microspheres obtained at 150 °C for 12 h, (b) hollow core-shell α -Fe₂O₃ microspheres obtained at 200 °C for 12 h, between voltage limits of 0.1-3.0 V at a current density of 150 mA g⁻¹.

Fig. 10 further compares the cycling performance of the hollow core-shell α -Fe₂O₃ microspheres and the solid α -Fe₂O₃ microspheres within sixty cycles. A much higher reversible capacity of the hollow core-shell α -Fe₂O₃ microspheres is 728 mAh g⁻¹, which is higher than the solid microspheres (358 mAh g⁻¹) for up to 60 cycles of discharge/charge. It is clear that the hollow core-shell α -Fe₂O₃ microspheres manifest a significantly enhanced cycling performance compared to its solid counterpart. The enhanced lithium storage properties can be attributed to the unique hollow mesoporous structure, where the hollow mesoporous structure can offer better electrolyte accessibility and buffer the volume change during the charge-discharge processes, which can effectively accommodate a larger degree of structural deformation during Li insertion/extraction [33, 34]. Furthermore, this porous core-shell structure provides larger specific surface areas, leading to an increased number of electrochemically active surface preventing the active materials from falling off the current collector [35]. The results indicate that the hollow core-shell α -Fe₂O₃ microspheres can largely improve the electrochemical performance of lithium ion batteries.

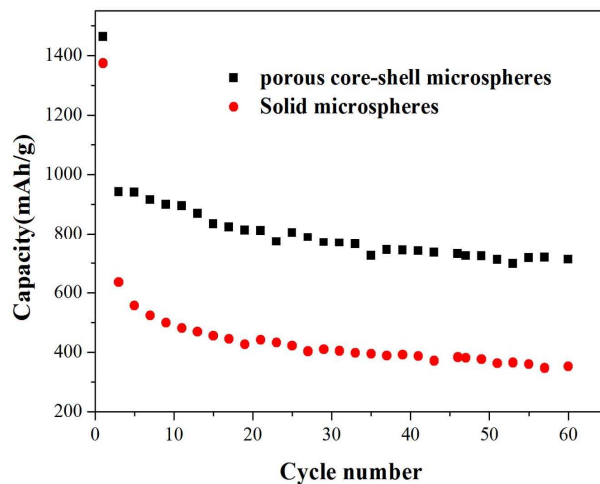


Fig. 10 Cycling performance of the hollow core-shell α -Fe₂O₃ microspheres and the solid α -Fe₂O₃ microspheres.

α -Fe₂O₃ has been widely used in the detection of combustible and noxious gases in air because it is an n-type semiconductor with an electrical conductivity highly sensitive to the gaseous environment [36–38]. Inspired by that, it was supposed that the hollow core-shell α -Fe₂O₃ microspheres have great potential in gas detection. Selectivity is very important to a gas sensor. The poor selectivity will induce mistaken alarm. Fig. 11 presents a bar graph of the sensitivity of the hollow core-shell α -Fe₂O₃ and the solid α -Fe₂O₃ sensors toward ten types of gases or vapors with a concentration of 50 ppm at 285 °C. The results indicated that both of the α -Fe₂O₃ sensor exhibited an obvious selectivity to nitrogen dioxide (NO₂) as opposed to any other gas. Furthermore, the sensitivity of hollow core-shell α -Fe₂O₃ sensor was much higher than solid α -Fe₂O₃ sensor, which indicated the hollow core-shell α -Fe₂O₃ may be used to detect NO₂ gas. As we know, sensors based on hierarchically porous structures or hollow microspheres provide higher surface-to-volume ratios, with reduced tendency to form agglomerates due to their larger dimensions [39, 40]. This allows for fast and effective gas adsorption onto the entire sensing surface simultaneously,

improving sensitivity and response time. The sensitivity of the hollow core–shell α -Fe₂O₃ toward trace levels of ethanol (C₂H₅OH) gas was the half of literature data [41], perhaps because of the size of samples that we prepared were bigger, resulting specific surface area was relatively small.

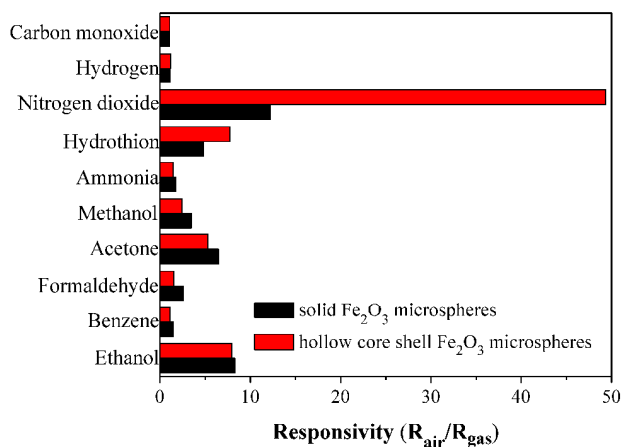


Fig. 11 Responses of the hollow core–shell α -Fe₂O₃ and solid α -Fe₂O₃ sensor to 50 ppm NO₂ at 285 °C.

In order to determine the optimal operating temperature, the sensitivity of the two α -Fe₂O₃ sensors toward 50 ppm of NO₂ were tested as function of operating temperature, as shown in Fig. 12. It is obvious that the hollow core–shell α -Fe₂O₃ sensors have much higher sensitivity than the solid α -Fe₂O₃ sensors in the whole temperature range from 160 to 355 °C. The results indicate that the sensitivities for hollow core–shell α -Fe₂O₃ microspheres increase with the temperature and reach its maximum of 50 at 285 °C, and then decrease rapidly with further rise of the operating temperature, while the sensitivities of solid α -Fe₂O₃ microspheres reach its maximum of 12.6 at 285 °C. Therefore, optimal operating temperature of 285 °C could be useful for an improved selectivity of sensor to NO₂.

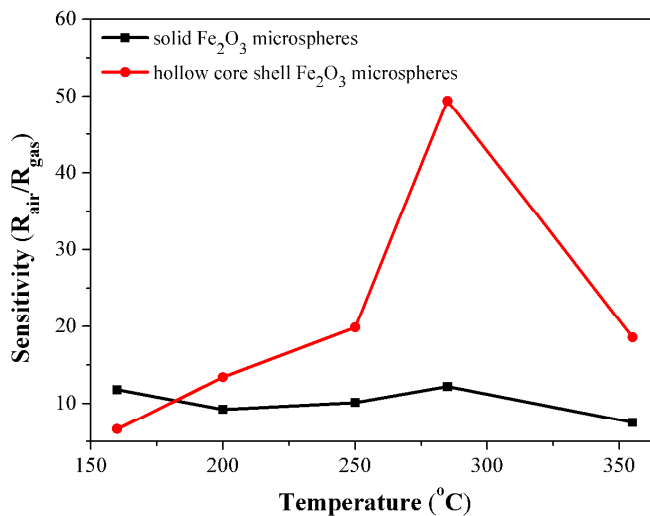


Fig. 12 Sensitivities of the hollow core-shell and solid α -Fe₂O₃ sensors to 50 ppm NO₂ at different operating temperatures.

The correlation between sensitivity and NO₂ concentrations for the two α -Fe₂O₃ sensor at operating temperature of 285 °C is displayed in Fig. 13 (a). When the NO₂ concentration is 5.0, 10, 20, 50, 100 and 200 ppm, respectively, the responding sensitivity of hollow core-shell α -Fe₂O₃ is 6.0, 7.3, 25.2, 49.5, 75.3 and 133.5, while that of solid α -Fe₂O₃ is 2.3, 2.7, 6.8, 12, 13.7 and 17 under the same conditions. Above 50 ppm, the sensitivity is nearly linear, and increase slowly with increasing NO₂ concentration, which indicates the gradually saturation of the adsorbed oxygen on the limited adsorption sites. It was noted that hollow core-shell α -Fe₂O₃ displayed a much higher sensitivity than the solid α -Fe₂O₃ toward NO₂. Fig. 13 (b, c) shows the dynamic response-recovery curves for the sensors based on the hollow core-shell and solid α -Fe₂O₃ microspheres at different concentrations of NO₂ at operating temperature of 285 °C. Six testing cycles were recorded, corresponding to six different NO₂ concentrations from 5 to 200 ppm, respectively. It can be seen that the values of the output voltage increased abruptly after the injection of NO₂ and

recovered their initial values after test gas was released. Response-recovery times of the hollow core-shell α -Fe₂O₃ microspheres and solid α -Fe₂O₃ microspheres calculated from the case of 50 ppm are 4-30 s and 7-30 s, respectively, indicating the hollow core-shell α -Fe₂O₃ microspheres exhibit much quicker response-recovery time. The superior sensitivity of the hollow core-shell α -Fe₂O₃ microspheres could be attributed to the unique core-shell structure with the interior space and the pores in the core, which provides abundant space and active sites for the adsorption of gases and reaction between adsorbed oxygen ions and detected gases.

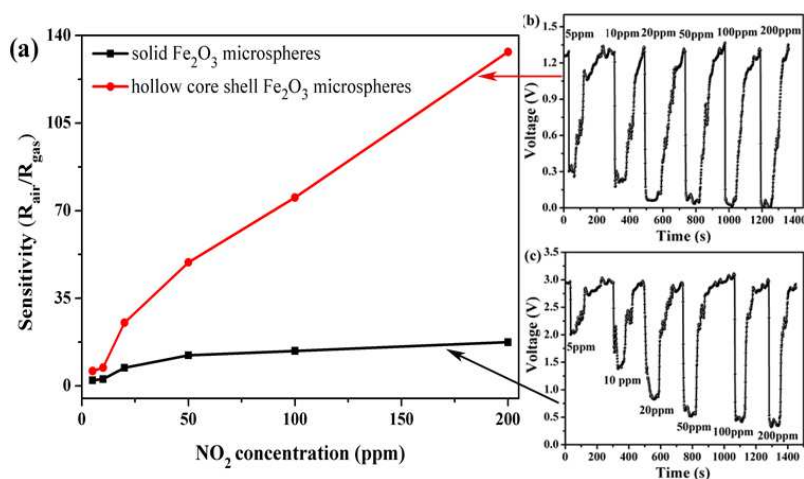


Fig. 13 (a) the sensors sensitivity of the as-prepared hollow core-shell α -Fe₂O₃ microsphere and solid α -Fe₂O₃ microsphere with different NO₂ concentrations at 285 °C; Dynamic response-recovery curves of the sensors based on the hollow core-shell (b) and solid (c) α -Fe₂O₃ microspheres to 5-200 ppm NO₂ at 285 °C.

For the sensing mechanism of semiconductor oxide gas sensor, the most widely accepted theory is based on the change in resistance of the sensor by the adsorption and desorption process of oxygen molecules on the surface of sensing materials [42–45]. In the ambient environment, oxygen molecules are adsorbed on the surface of the n-type α -Fe₂O₃. The adsorbed O₂ captured electrons from the conduction band

of the α -Fe₂O₃ semiconductor to form adsorbed oxygen ions and increase the resistance of the α -Fe₂O₃ sensor, due to the lower concentration of free electrons in the materials conduction band. When the sensor is exposed to oxidizing gas such as NO₂, the test gas molecules are chemi-adsorbed at the active sites on the surface of the as-prepared hollow core-shell α -Fe₂O₃ microspheres. These NO₂ molecules will be reduced by the adsorbed oxygen ions. During this reduction process, the adsorbed oxygen will continue to trap electrons from the surface of the as-prepared α -Fe₂O₃ sensor to higher the number of trapped electrons, which induced an increase in the measured resistance.

4. Conclusions

In summary, the hollow core-shell α -Fe₂O₃ microspheres have been successfully fabricated by one-pot facile and template-free hydrothermal route. With such a unique porous core-shell structure, the hollow core-shell α -Fe₂O₃ microspheres have potential applications in Li-storage and gas-sensing performance. As a Li-storage anode material for Li-ion battery, the hollow core-shell α -Fe₂O₃ microspheres exhibit a higher charge/discharge capacity and better cyclic performance than the solid α -Fe₂O₃ microspheres, which shows a higher discharge specific capacity of 1465 mAh g⁻¹ for the first cycle and 728 mAh g⁻¹ after 60 cycles. The application in gas sensors reveals that the hollow core-shell α -Fe₂O₃ microspheres show high gas sensitivity toward NO₂ gas and short response/recovery time. The strategy adopted in this work is expected to be broadly employed for fabrication of many types of advanced materials with the varying composite structures, which may have more efficient and

practical applications in the fields of energy and environment.

Acknowledgements

We gratefully acknowledge the support of the National Natural Science Foundation of China (No. 51372103 and 51202092), and the financial support from China Scholarship Council (201308320062).

References

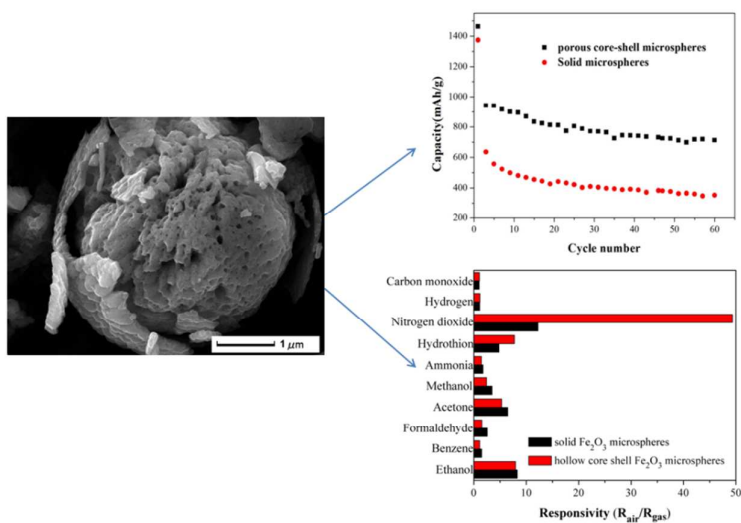
- 1 J. Xu, F. Huang, Y. L. Yu, A. P. Yang and Y. S. Wang, *CrystEngComm*, 2011, **13**, 4873–4877.
- 2 S. Yang, Y. Y. Xu, Y. Q. Sun, G. Y. Zhang and D. Z. Gao, *CrystEngComm*, 2012, **14**, 7915–7921.
- 3 J. R. Huang, M. Yang, C. P. Gu, M. H. Zhai, Y. F. Sun and J. H. Liu, *Mater. Res. Bull.*, 2011, **46**, 1211–1218.
- 4 M. Mahmoudi, A. Simchi and M. Imani, *J. Iran, Chem. Soc.*, 2010, **7**, S1–S27.
- 5 T. E. García, M. Valvo, U. Lafont, C. Locati, D. Munao and E. M. Kelder, *J. Power Sources*, 2011, **196**, 6425–6432.
- 6 T. P. Almeida, M. W. Fay, T. W. Hansen, Y. Q. Zhu and P. D. Brown, *CrystEngComm*, 2014, **16**, 1540–1546.
- 7 X. H. Rao, X. T. Su, C. Yang, J. D. Wang, X. P. Zhen and D. S. Ling, *CrystEngComm*, 2013, **15**, 7250–7256.
- 8 J. Chen, L. N. Xu, W. Y. Li and X. L. Gou, *Adv. Mater.*, 2005, **17**, 582–586.
- 9 M. V. Reddy, T. Yu, C. H. Sow, Z. X. Shen, C. T. Lim, G. V. S. Rao and B. V. R.

- Chowdari, *Adv. Funct. Mater.*, 2007, **17**, 2792–2799.
- 10 J. S. Xu and Y. J. Zhu, *CrystEngComm*, 2011, **13**, 5162–5169.
- 11 J. S. Xu and Y. J. Zhu, *CrystEngComm*, 2012, **14**, 2702–2710.
- 12 S. W. Cao, Y. J. Zhun, G. F. Cheng and Y. H. Huang, *J. Phys. Chem. Solids*, 2010, **71**, 1680–1683.
- 13 S. H. Yu, Q. Z. Yao, G. T. Zhou, and S. Q. Fu, *ACS Appl. Mater. Interfaces*, 2014, **6**, 10556–10565.
- 14 Z. C. Wu, K. Yu, S. D. Zhang and Y. Xie, *J. Phys. Chem. C*, 2008, **112**, 11307–11313.
- 15 X. Y. Zhao, M. H. Cao and C. W. Hu, *Mater. Res. Bull.*, 2013, **48**, 2289–2295.
- 16 Y. T. Wu and X. F. Wang, *Mater. Lett.*, 2011, **65**, 2062–2065.
- 17 A. Abdi and M. Trari, *Electrochim. Acta.*, 2013, **111**, 869–875.
- 18 L. Wang, H. W. Xu, P. C. Chen, D. W. Zhang, C. X. Ding and C. H. Chen, *J. Power Sources*, 2009, **193**, 846–850.
- 19 J. B. Lian, X. C. Duan, J. M. Ma, P. Peng, T. I. Kim and W. J. Zheng, *ACS Nano.*, 2009, **3**, 3749–3761.
- 20 F. Y. Cheng, Z. L. Tao, J. Liang and J. Chen, *Chem. Mater.*, 2008, **20**, 667–681.
- 21 M. Llusar, V. Royo, J. A. Badenes, M. A. Tena and G. Monrós, *J. Eur. Ceram. Soc.*, 2009, **29**, 3319–3332.
- 22 J. Wang, Y. Bai, M. Wu, J. Yin and W. Zhang, *J. Power Sources*, 2009, **191**, 614–618.
- 23 J. H. Bang and K. S. Suslick, *J. Am. Chem. Soc.*, 2007, **129**, 2242–2243.

- 24 H. Qian, G. Lin, Y. Zhang, P. Gunawan and R. Xu, *Nanotechnology*, 2007, **18**, 355602–355608.
- 25 J. Y. Zhong, C. B. Cao, Y. Y. Liu, Y. N. Li and W. S. Khan, *Chem. Commun.*, 2010, **46**, 3869–3871.
- 26 X. L. Hu and J. C. Yu, *Adv. Funct. Mater.*, 2008, **18**, 880–887.
- 27 J. R. Huang, M. Yang, C. P. Gu, M. H. Zhai, Y. F. Sun and J. H. Liu, *Mater. Res. Bull.*, 2011, **46**, 1211–1218.
- 28 M. Zic, M. Risti and S. Music, *J. Alloys Compd.*, 2008, **464**, 81–88.
- 29 X. L. Fang, C. Chen, M. S. Jin, Q. Kuang, Z. X. Xie, S. Y. Xie, R. B. Huang and L. S. Zheng, *J. Mater. Chem.*, 2009, **19**, 6154–6160.
- 30 X. J. Wang, F. Q. Wan, Y. J. Gao, J. Liu and K. J. Jiang, *Cryst Growth* 2008, **310**, 2569–2576.
- 31 Y. Z. Lei, J. C. Hu, H. W. Liu and J. L. Li, *Mater. Lett.*, 2012, **68**, 82–85.
- 32 L. Y. Nu, P. Zhang, Z. P. Guo and H. Liu, *J. Electrochem. Soc.*, 2008, **155**, A196–A200.
- 33 K. A. Kwon, H. S. Lim, Y. K. Sun and K. D. Suh, *J. Phys. Chem. C*, 2014, **118**, 2897–2907.
- 34 J. Zhang, Y. Sun, Y. Yao, T. Huang and A. Yu, *J. Power Sources*, 2013, **222**, 59–65.
- 35 J. P. Liu, Y. Y. Li, X. T. Huang, R. M. Ding, Y. Y. Hu, J. Jiang and L. J. Liao, *J. Mater. Chem.*, 2009, **19**, 1859–1864.
- 36 P. Sun, W. N. Wang, Y. P. Liu, Y. F. Sun, J. Ma and G. Y. Lu, *Sens. Actuators, B*

- 2012, **173**, 52–57.
- 37 C. H. Zhao, W. Q. Hu, Z. X. Zhang, J. Y. Zhou, X. J. Pan and E. Q. Xie, *Sens. Actuators, B* 2014, **195**, 486–493.
- 38 S. M. Liang, J. W. Zhu, C. Wang, S. T. Yu, H. P. Bi, X. H. Liu and X. Wang, *Appl. Surf. Sci.*, 2014, **292**, 278–284.
- 39 A. Gurlo, *Nanoscale*, 2011, **3**, 154–165.
- 40 X. Wang, W. Liu, J. Liu, F. Wang, J. Kong, S. Qiu, C. He and L. Luan, *ACS Appl. Mater. Interfaces*, 2012, **4**, 817–825.
- 41 Z. C Wu, K. Yu, S. D. Zhang, and Y. Xie, *J. Phys. Chem. C* 2008, **112**, 11307–11313.
- 42 J. Q. Xu, J. J. Han, Y. Zhang, Y. A. Sun and B. Xie, *Actuators, B* 2008, **132**, 334–339.
- 43 K. Wetchakun, T. Samerjai, N. Tamaekong, C. Liewhiran, C. Siriwong, V. Kruefu, A. Wisitsoraat, A. Tuantranont and S. Phanichphant, *Sens. Actuators, B* 2011, **160**, 580–591.
- 44 J. Zhao, T. L. Yang, Y. P. Liu, Z. Y. Wang, X. W. Li, Y. F. Sun, Y. Du, Y. C. Li and G. Y. Lu, *Sens. Actuators, B* 2014, **191**, 806–812.
- 45 A. Sharma, M. Tomar and V. Gupta, *Sens. Actuators, B* 2013, **181**, 735–742.

Graphical abstract



The hollow core-shell α -Fe₂O₃ microspheres with improved lithium storage and gas-sensing properties have been fabricated by the template-free hydrothermal route.